Optimization of Random Surface Scattering Models for RR Polarization in SoOp-R/GNSS-R Applications

Xuerui Wu, Lixiong Chen, and Jiancheng Shi, *Fellow, IEEE*

***Abstract*—Polarization in global navigation satellite system-reflectometry (GNSS-R) or signal of opportunity-reflectometry (SoOP-R) is commonly used for retrieving geophysical parameters. However, the attention toward other polarizations of reflected signals has increased with developments in this field. The widely used equation for RR polarization suggests that it decreases as soil moisture content increases, which contradicts the experimental data. The accurate forward calculation of RR polarization is essential for the subsequent retrieval algorithm in polarization GNSS-R/SoOP-R. To address this issue, three new models have been developed: specular reflectivity model for polarization GNSS-R (Spec4PolR), small perturbation model for polarization GNSS-R (SPM4Pol), and Umich model for polarization GNSS-R (Umich4PolR). The Mueller matrix of these three models has been presented, and the wave synthesis technique has been employed to calculate the reflectivity at RR polarization. Spec4polR uses only three elements in the Mueller matrix for final reflectivity, while five elements are used in Umich4polR. In SPM4Pol, all elements construct the Mueller matrix, and only nine elements are employed for calculation. The effects of each element on soil moisture content are presented, and the final reflectivity at RR polarization is illustrated. However, due to the simple formulation of Spec4Pol, its reflectivity at RR polarization still decreases as soil moisture content increases. On the other hand, the results of SPM4Pol and Umich4Pol are consistent with the measured data, and the reflectivity at RR polarization increases as soil moisture content increases. The formula developed in this article for calculating RR polarization will contribute to subsequent polarization studies and geophysical parameter retrieval based on RR polarization.**

***Index Terms*—Global navigation satellite system-reflectometry (GNSS-R)/signal of opportunity-reflectometry (SoOP-R), random rough surface scattering model, RR polarization, specular reflectivity.**

I. Introduction

THE retrieval of global geophysical parameters at large spatiotemporal scales is a requirement for the Earth science community, and signals of opportunity (SoOp) based systems have recently emerged as a novel microwave remote sensing domain.

Manuscript received 17 October 2023; revised 5 December 2023; accepted 20 January 2024. Date of publication 15 February 2024; date of current version 22 February 2024. This work was supported in part by the National Natural Science Foundation of China under Grant 42061057 and in part by the Key Laboratory Fund for Key Laboratory of Satellite Navigation Technology. *(Corresponding author: Xuerui Wu.)*

Xuerui Wu is with Shanghai Astronomical Observatory, Chinese Academy of Sciences, Shanghai 200030, China (e-mail: xrwu@shao.ac.cn).

Lixiong Chen is with Shanghai Maritime University, Shanghai 200030, China (e-mail: chenlixiong2002@163.com).

Jiancheng Shi is with National Space Science Centers, Chinese Academic of Sciences, Beijing 100190, China (e-mail: shijiancheng@nssc.ac.cn).

Digital Object Identifier 10.1109/JSTARS.2024.3361923

The signal of opportunity-reflectometry (SoOP-R) approach's main principle is to receive and further extract information from free illuminators whose signal reflects off the Earth's surface. In contrast to the traditional microwave remote sensing, the existing signal sources are used in a bistatic configuration with the transmitter and receiver separated by a considerable distance [1], [2], [3].

Since the 1990s, the SoOP-R concept has been extensively used for collecting or modeling the global navigation satellite system (GNSS) signal reflections over the ocean surface to estimate wind vectors [4], [5], [6], [7], [8].

Later on, its applications on land surfaces have emerged and become more and more promising, such as soil moisture or root zone soil moisture estimation [9], [10], vegetation water content or biomass retrieval [11], [12], and snow water equivalent evaluation [13] by SoOP-R or global navigation satellite system-reflectometry (GNSS-R).

As an emerging remote sensing method, SoOP-R/GNSS-R essentially utilizes sensors to detect the scattering and reflection characteristics of electromagnetic waves from objects. Polarization is an important characteristic of electromagnetic waves defined as the variation of the electric field trajectory over time at a certain position.

In the initial GNSS-R study, it was believed that navigation satellites emitted right-handed circularly polarized (RHCP) signals. Due to the weak signal energy reflected from the surface, it is necessary to use left-handed circularly polarized (LHCP) signals to effectively isolate the impact of direct signals and study the reflection characteristics of ground objects [14]. Regardless of whether in the ocean or land domain, the focus is on LR (the transmitted signals are RHCP, while the received ones are LHCP) polarization, that is to say, researchers have to invert surface parameters using LR polarization reflected signals [15], [16], [17], [18].

However, with the development of GNSS-R technology, the exploration and analysis of its other polarization characteristics have never stopped. For example, in the monitoring of soil moisture on the land surface, the receiver of the BAO tower in situ measurement uses antennas with different polarizations to measure the surface reflection signal, and then analyzes the sensitivity of various polarizations to soil moisture, a low-gain RHCP antenna in the receiver antenna that points toward the zenith to receive direct signals; five receiver antennas pointing toward the ground: 1 low-gain LHCP, 4 high-gain (approximately 12 dB) antennas, i.e., V, H, RHCP, and LHCP [19]. One important point that should be mentioned is that the experimental

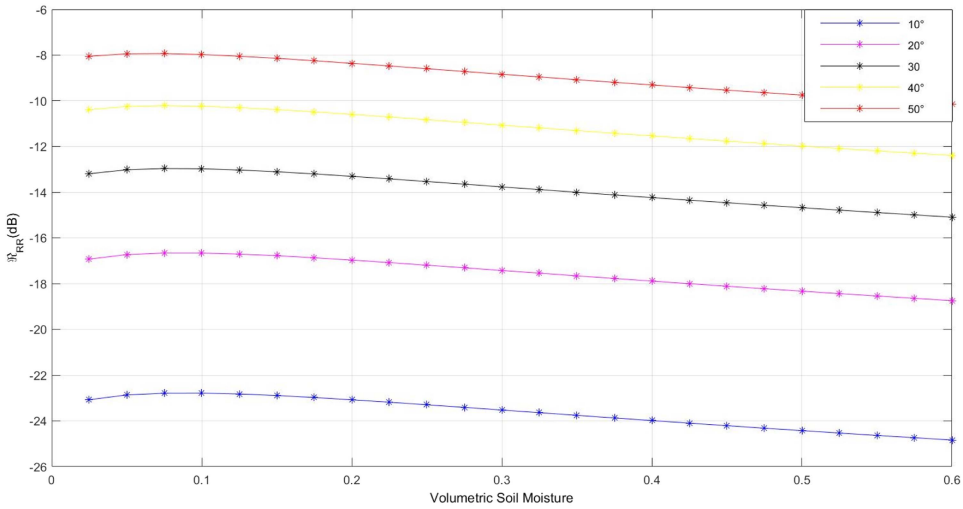

Fig. 1. Reflectivity of RR polarization versus soil moisture at different incidence angles.

results are inconsistent with the theoretical model results due to the simplistic assumption of the model.

On satellite receivers, the antennas of United Kingdom-Disaster Monitoring Constellations, cyclone global navigation satellite system (CYGNSS), and F3E GNSS occultation sounder II-reflectometry receivers are all LR polarization, and several results have been achieved in the inversion of wind speed, sea wave height, soil moisture, and vegetation biomass [11], [12], [15], [16], [17], [18].

Using a combination of *L*-band radiometry and SAR, the soil moisture active passive (SMAP) mission was launched in 2015 with the objective of studying the Earth's surface properties, soil moisture, and freeze/thaw being its primary objectives. Shortly after its launch, the radar was directed to stop its normal activities, while the SMAP radar receiver was adjusted to catch up with GPS *L*2 reflected signals, and we call this SMAP-reflectometry (SMAP-R), which is a special polarimetric GNSS-R. Furthermore, the computation of the signal's Stokes parameters allows for full reconstruction and a better understanding of the polarimetric properties of the received signal. With the polarimetric SMAP-R data, not only reflectivity at LR pol but also reflectivity at RR (the transmitted signals and the received ones are all RHCP polarization), VR (the transmitted signals are RHCP polarization, while the received ones are vertical polarization), and HR (the transmitted signals are RHCP polarization, while the received ones are horizontal polarization) polarization was used for the final soil moisture or surface roughness estimation [20], [21].

Before the end of 2024, HydroGNSS, which has been chosen as the second scout small satellite mission, will be built and launched. Different from the previous CYGNSS, one unique feature of HydroGNSS is its polarization. DDMs will be gathered from the antenna's left- and right-hand circular polarizations. The ratio of the two polarizations (RR/LR) can assist in distinguishing soil roughness effects from soil wetness, as well as in distinguishing biomass from ground reflections [22].

We can see that different from the traditional research on LR polarization characteristics, using RR polarization to study ground features is an important research method, and the study of RR polarization characteristics is an inevitable trend for the development of polarimetric GNSS-R. Therefore, the study of the mechanism model of RR polarization is particularly important [23], [24], [25].

The rest of this article is organized as follows. The theoretical fundamentals' models are presented in Section II, and Section III provides the numerical simulation results. Finally, Section IV discusses and concludes this article.

II. Theoretical Fundamentals

In this section, we will present the theoretical fundamentals for random surface scattering models of RR polarization.

For an ideal smooth surface, the reflectivity is determined by the Fresnel reflection coefficient and the polarization mode of the incident signals [27]. The Fresnel reflection coefficients for horizontal and vertical polarizations are as follows:

$$r_h = \frac{\cos\theta - \sqrt{\varepsilon_r - \sin^2\theta}}{\cos\theta + \sqrt{\varepsilon_r - \sin^2\theta}} \tag{1}$$

$$r_v = \frac{\varepsilon_r \cos\theta - \sqrt{\varepsilon_r - \sin^2\theta}}{\varepsilon_r \cos\theta + \sqrt{\varepsilon_r - \sin^2\theta}}. \tag{2}$$

While θ is the incidence angle, ε_r is the complex dielectric constant, and the subscripts h and v demonstrate the polarization states.

For completely smooth surfaces, the cross-polarization term r_{hv} and r_{hv} can be ignored. For GNSS signals, the satellite transmission signal is RHCP, which can be understood as a linear combination of horizontal and vertical polarization components [14]

TABLE I
VALUES OF ψ, χ, AND THE NORMALIZED STOKES PARAMETERS $i_v = I_v/I_0$, $i_h = I_h/I_0$, $u = U/I_0$, AND $v = V/I_0$ FOR SOME COMMONLY USED POLARIZATION STATES

Polarization State	Rotation Angle (ψ)	Ellipticity Angle (χ)	Nor.Stokes Parameters			
			i_v	i_h	u	v
Vertical	0°	0°	1	0	0	0
Horizontal	90°	0°	0	1	0	0
Right circular	–90°to 90°	–45°	1/2	1/2	0	–1
Left circular	–90°to 90°	45°	1/2	1/2	0	1

$$\Gamma_{rr} = \frac{1}{2}\left(r_{vv} + r_{hh}\right) = \frac{\left(\varepsilon_r - 1\right)^2 \sin^4\theta}{\left(\varepsilon_r \sin\theta + \sqrt{\varepsilon_r - \sin^2\theta}\right)^2 \left(\cos\theta + \sqrt{\varepsilon_r - \sin^2\theta}\right)^2} \tag{3}$$

where (3) is the commonly used formula to calculate the specular reflectivity at RR polarization, and its relationship with soil moisture content is demonstrated in Fig. 1.

The variations of reflectivity at RR polarization versus soil moisture content at different incidence angles (10°, 20°, 30°, and 65°) are presented in Fig. 1. From the simulations, it can be seen that the simulated reflectivity using (3) decreases with increasing soil moisture. However, both the BAO tower experiment and soil moisture monitoring station in situ measurement indicate that the reflectivity of RR polarization increases with soil moisture contents [19], [28]. Therefore, there is a contradiction between the results obtained from (3) and the in situ measured data.

A. Wave Synthesis Technique

In order to solve the problems, we will provide three models for evaluation in this section. Since we want to calculate the specular reflectivity at RR polarization, we will employ the wave synthesis technique to get the polarization properties [29].

The electric field can be represented by an E-vector with components E_v and E_h, both of them represent the vertical polarization component E_v and the horizontal polarization component E_h

$$E = \begin{bmatrix} E_v \\ E_h \end{bmatrix}. \tag{4}$$

One set of parameters for characterizing polarization state is Stokes' representation, which consists of four Stokes parameters, I_0, Q, U, and V. I_0 represents the total intensity of the wave, Q represents the difference between vertically polarized intensity and the horizontally polarized intensity, and the last two (U and V) represent jointly the phase difference between the vertically polarized and horizontally polarized components of the wave

$$I_0^2 = Q^2 + U^2 + V^2. \tag{5}$$

While Q, U, and V are the functions of ellipticity angle and rotation angle. The definition of modified Stokes vector can be defined as

$$F_m = \begin{bmatrix} I_v \\ I_h \\ U \\ V \end{bmatrix} = \begin{bmatrix} \frac{1}{2}\left(1 + \cos 2\psi \cos 2\chi\right) \\ \frac{1}{2}\left(1 - \cos 2\psi \cos 2\chi\right) \\ \sin 2\psi \cos 2\chi \\ \sin 2\chi \end{bmatrix} \tag{6}$$

$$I_v = |E_v|^2 = (I_0 + Q)/2 \tag{7}$$

$$I_h = |E_h|^2 = (I_0 - Q)/2. \tag{8}$$

It should be mentioned that by changing the ellipticity angle and rotation angle, we can get the reflectivity at any polarization combination. Table I presents the defined angles for the commonly used polarization state. The corresponding normalized Stokes parameters are also presented.

The scattered wave Stokes vector can be connected to the incident wave Stokes vector through the Mueller matrix

$$\overline{F}^r = \frac{1}{r^2}\overline{M}\left(\theta_s, \phi_s; \theta_i, \phi_i; \theta_j, \phi_j\right)\overline{F}^t. \tag{9}$$

Because the scattered wave is spherical, the factor $1/r^2$ is required. As for the calculation of RR polarization, after getting the modified Stokes vectors, as shown in Table I, the other important step is to calculate the Mueller matrix, which will be presented in the parts B, C, and D of this section.

B. Specular Reflectivity Model for Polarization GNSS-R (Spec4PolR)

We will employ the specular reflectivity matrix to calculate the reflectivity at RR polarization, while this model is named Spec4PolR. All the elements in this model are based on the Fresnel reflectivity (r_v and r_h) at vertical polarization and horizontal polarization, as shown in (1) and (2).

The reflectivity matrix of a specular ground surface, which is directly related to the Mueller matrix, can be defined as follows [30]:

$$\Re\left(\theta\right) = \begin{bmatrix} |r_v|^2 & 0 & 0 & 0 \\ 0 & |r_h|^2 & 0 & 0 \\ 0 & 0 & \mathrm{Re}\left(r_v r_h^*\right) & -\mathrm{Im}\left(r_v r_h^*\right) \\ 0 & 0 & \mathrm{Im}\left(r_v r_h^*\right) & \mathrm{Re}\left(r_v r_h^*\right) \end{bmatrix}. \tag{10}$$

To simplify the final form and demonstrate the elements that calculate the final Mueller matrix, we will employ the following

equation and is a real $4 * 4$ matrix

$$S = \begin{bmatrix} S_{11} & 0 & 0 & 0 \\ 0 & S_{22} & 0 & 0 \\ 0 & 0 & S_{33} & S_{34} \\ 0 & 0 & S_{43} & S_{44} \end{bmatrix}. \tag{11}$$

We can see that there are six elements for the final Mueller matrix and they are S_{11}, S_{22}, S_{33}, S_{34}, and S_{43}. After multiplying modified Stokes vectors and their transform formation at the left side and right side of the Mueller matrix, respectively, we can get the below equation to calculate the final reflectivity.

$$\sigma^0_{Spec-PolR} = \frac{1}{4}S_{11} + \frac{1}{4}S_{22} - \frac{1}{2}S_{44} = \frac{1}{4}|r_v|^2 + \frac{1}{4}|r_h|^2 - \frac{1}{2}\mathrm{Re}\left(r_v r_h^*\right) \tag{12}$$

It should be mentioned from the above equation that only three elements of the Mueller matrix are used for the final calculation, e.g., S_{11}, S_{22}, and S_{44}, while S_{33}, S_{34}, and S_{43} are not employed for the final calculation. Different from the previously used equations, in the modified equations, one-quarter of the modulus of r_v and r_h and a half of the real part of r_v and r_h^* participate in the final calculations.

C. Umich Model for Polarization GNSS-R (Umich4PolR)

Umich model is an empirical model developed based on polarimetric radar measurement [32]. Here, it has been employed for the calculation of specular reflectivity at RR polarization. And the developed model is named Umich4PolR. The copolarization and cross-polarization scattering coefficients at *vv*, *hh*, and *hv* are as follows:

$$\sigma^o_{vv}(\theta, \varepsilon_r, ks) = \frac{g\cos^3\theta}{\sqrt{p}} \cdot \left[\Gamma_v(\theta) + \Gamma_h(\theta)\right] \tag{13}$$

$$\sigma^o_{hh}(\theta, \varepsilon_r, ks) = g\sqrt{p}\cos^3\theta \cdot \left[\Gamma_v(\theta) + \Gamma_h(\theta)\right] \tag{14}$$

$$\sigma^o_{hv}(\theta, \varepsilon_r, ks) = q\sigma^o_{vv}(\theta, \varepsilon_r, ks). \tag{15}$$

θ, ε_r, and ks are the incidence angle, dielectric constant, and surface roughness, respectively.

While the formula of q can be expressed as follows:

$$q \triangleq \frac{\sigma^o_{hv}}{\sigma^o_{vv}} = 0.23\sqrt{\Gamma_0}\left[1 - \exp(-ks)\right] \tag{16}$$

where Γ_0 is the Fresnel reflectivity of the surface at the nadir direction

$$\sqrt{\Gamma_0} = \left|\frac{1 - \sqrt{\varepsilon_r}}{1 + \sqrt{\varepsilon_r}}\right|^2 \tag{17}$$

$$\sqrt{p} \triangleq \sqrt{\frac{\sigma^o_{hh}}{\sigma^o_{vv}}} = 1 - \left(\frac{2\theta}{\pi}\right)^{[1/3\Gamma_0]} \cdot \exp(-ks). \tag{18}$$

The *W* matrix that is used to calculate the Mueller matrix is given in 19, while its basic elements can be summarized based on σ^o_{vv}, σ^o_{hh}, and σ^o_{hv}

$$WW = \begin{bmatrix} \left(\sigma^0_{vv}\right)^2 & \left(\sigma^0_{hv}\right)^2 & 0 & 0 \\ \left(\sigma^0_{hv}\right)^2 & \left(\sigma^0_{hh}\right)^2 & 0 & 0 \\ 0 & 0 & \sigma^2_{hh}\sigma^2_{vv} & 0 \\ 0 & 0 & 0 & \sigma^2_{hh}\sigma^2_{vv} \end{bmatrix}. \tag{19}$$

The final form for the Mueller matrix of the Umich4PolR model can be summarized as

$$U = \begin{bmatrix} U_{11} & U_{12} & 0 & 0 \\ U_{21} & U_{22} & 0 & 0 \\ 0 & 0 & U_{33} & 0 \\ 0 & 0 & 0 & U_{44} \end{bmatrix}. \tag{20}$$

After multiplying modified Stokes vectors at both sides of the Mueller matrix, we can get the final equations that are used to calculate the specular reflectivity at RR polarization

$$\sigma^0_{\text{Umich}} = \frac{1}{4}U_{11} + \frac{1}{4}U_{21} + \frac{1}{4}U_{12} + \frac{1}{4}U_{22} - \frac{1}{2}U_{44}. \tag{21}$$

Five elements in the matrix, as presented in (20), have been employed for the final calculation. It should be mentioned that the element of U_{33} is not employed for calculation.

D. SPM4PolR

The small perturbation model (SPM) is a commonly used model for computing the scattering from a natural surface [31]. Here, it will be developed and based on the wave synthesis technique to get the specular reflectivity at RR polarization and the developed model is named SPM4PolR.

The average modified Mueller matrix of the SPM model can be written as the function of polarization-dependent factors

$$\overline{M}_m = U_0\tilde{V}^{-1}\begin{bmatrix} f_{vv}f^*_{vv} & f_{vh}f^*_{vh} & f_{vv}f^*_{vh} & f_{vh}f^*_{vv} \\ f_{hv}f^*_{hv} & f_{hh}f^*_{hh} & f_{hv}f^*_{hh} & f_{hh}f^*_{hv} \\ f_{vv}f^*_{hv} & f_{vh}f^*_{hh} & f_{vv}f^*_{hh} & f_{vh}f^*_{hv} \\ f_{hv}f^*_{vv} & f_{hh}f^*_{vh} & f_{hv}f^*_{vh} & f_{hh}f^*_{vv} \end{bmatrix} V^{-1}. \tag{22}$$

While as for the SPM model, we can see that all the elements in the $4 * 4$ real matrix have their own definition and values. To simplify the expressions, we will employ *P* matrix to represent every element in the Mueller matrix and the final form for the Mueller matrix can be defined as follows:

$$P = \begin{bmatrix} P_{11} & P_{12} & P_{13} & P_{14} \\ P_{21} & P_{22} & P_{23} & P_{24} \\ P_{31} & P_{32} & P_{33} & P_{34} \\ P_{41} & P_{42} & P_{43} & P_{44} \end{bmatrix}. \tag{23}$$

After multiplying the modified Stokes vectors at both sides of the Mueller matrix, we can get the final form of the specular reflectivity at RR polarization, which is shown in the below equation. It should be mentioned that nine elements in the modified Mueller matrix have been employed for the final calculation, i.e., P_{14}, P_{24}, P_{11}, P_{21}, P_{41}, P_{12}, P_{22}, P_{42}, and P_{44}

$$\begin{aligned} \sigma^0_{\text{SPM}} = & -\frac{1}{2}P_{14} - \frac{1}{2}P_{24} + \frac{1}{4}P_{11} + \frac{1}{4}P_{21} \\ & + \frac{1}{4}P_{41} + \frac{1}{4}P_{12} + \frac{1}{4}P_{22} + \frac{1}{4}P_{42} - \frac{1}{2}P_{44}. \end{aligned} \tag{24}$$

Not all of the elements in (23) are used for reflectivity at RR polarization.

III. Numerical Simulation Results

The numerical simulation results based on Spec4PolR, Umich4PolR, and SPM4PolR will be presented in this section; each element that affects the final reflectivity will also

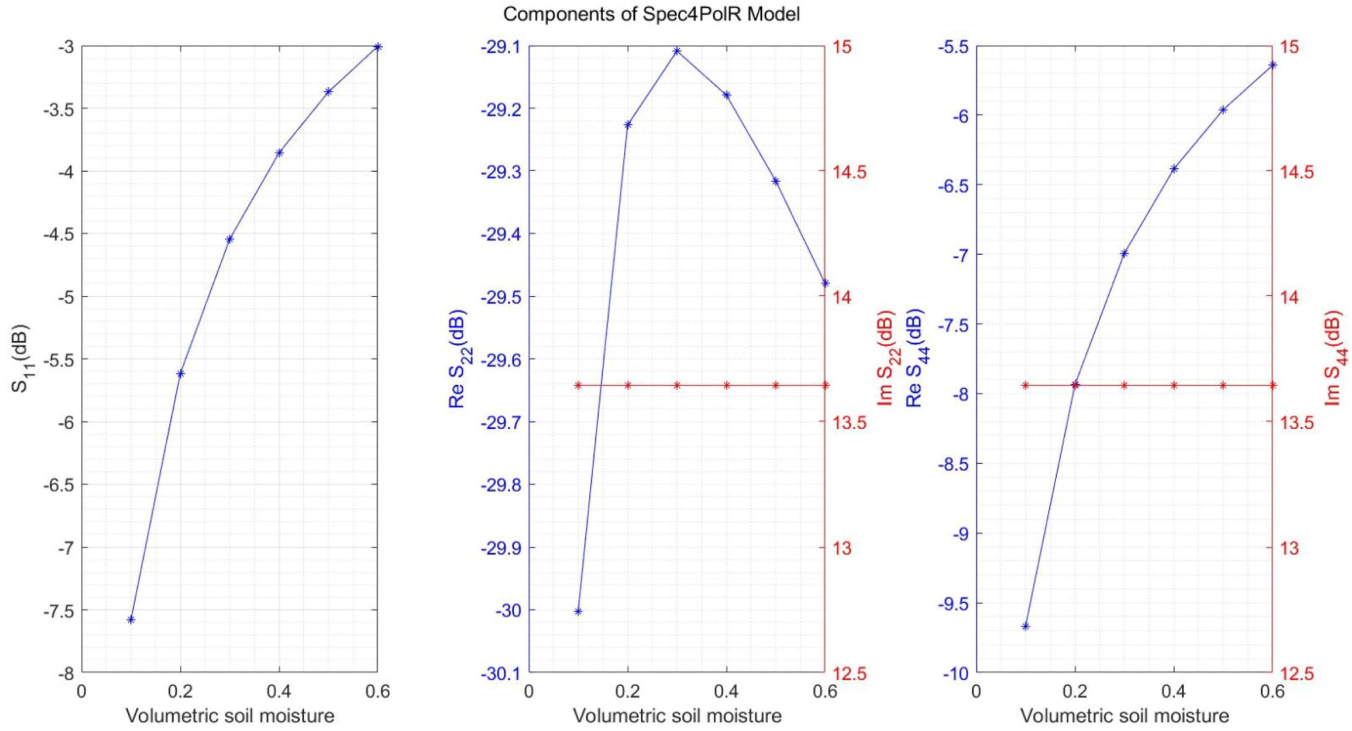

Fig. 2. Modified Mueller matrix elements of S_{11}, S_{22}, and S_{44} versus soil moisture content.

be presented and their effects on soil moisture content will be illustrated.

A. Spec4PolR

Spec4PolR is employed and its numerical simulation results are presented in this section. From (10) to (12), we can see that only the elements of S_{11}, S_{22}, and S_{44} in the $4 * 4$ real modified Mueller matrix are employed for the final RR reflectivity calculation; therefore, the relationship between the three elements versus the soil moisture contents is presented and simulated here. From the numerical simulations, as presented in Fig. 2, we can see that S_{11} increases as the soil moisture content increases. The real part of S_{22} increases as the soil moisture increases when the soil moisture content is below 0.3. However, if the soil moisture content is larger than 0.3, the real part of S_{22} decreases as the soil moisture content increases, and its imaginary part remains as a constant for different soil moisture contents. For S_{44} element, its real part increases as the soil moisture content increases, while the imaginary part remains as a constant during the variation of soil moisture content.

The left figure in Fig. 3 presents the RR scattering coefficient in the specular direction versus the soil moisture content. The soil moisture content for this simulation is 0.3, while the incidence angle is 30°. The final three elements in the Mueller matrix result that the RR reflectivity decreases as soil moisture content increases, while RR reflectivity increases as the specular incidence angle increases.

From the simulation, we can see that only three elements employed in the specular reflectivity matrix cannot be used for the accurate RR reflectivity calculation, that is to say, the Spec4PolR model cannot be used for RR calculations due to its simple utilization of the modified Mueller matrix elements.

B. Umich4PolR Model

Numerical simulation results of the Umich model for RR polarization GNSS-R application (Umich4PolR) are presented in this section. From (13) to (21), we can see that five elements (S_{11}, S_{21}, S_{12}, S_{22}, and S_{44}) are employed for the final RR reflectivity calculation. The five elements' effects on the soil moisture contents are the same: as the soil moisture contents increase, the five elements increase. Specular reflectivity at RR polarization is the result of the combined actions of five elements.

While the relationship between specular reflectivity at RR polarization with the soil moisture content is presented in the left figure of Fig. 5 and its relationship versus the specular incidence angles is presented in the right figure of Fig. 5.

From the left figure, we can see that, as the soil moisture content increases, the specular reflectivity at RR polarization increases. While as the incidence angle increases, the specular reflectivity at RR polarization increases. Both trends of Umich4PolR in Fig. 5 are consistent with the measured data.

C. SPM4PolR Model

The SPM model for RR polarization GNSS-R application (SPM4PolR) is presented in this section. The different element effects on soil moisture contents are presented and the final RR reflectivity versus soil moisture content and specular incidence angle are also illustrated in this section.

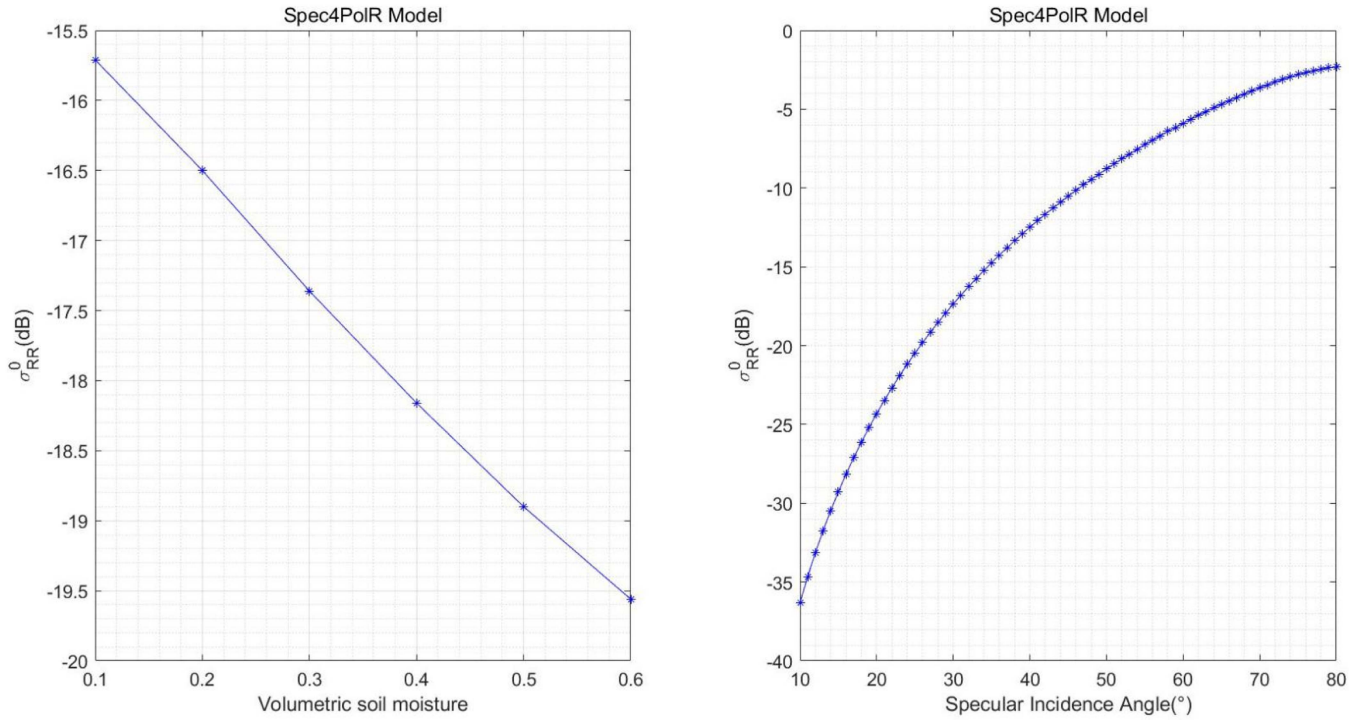

Fig. 3. Specular reflectivity at RR polarization versus soil moisture content (left figure) and specular incidence angle (right figure).

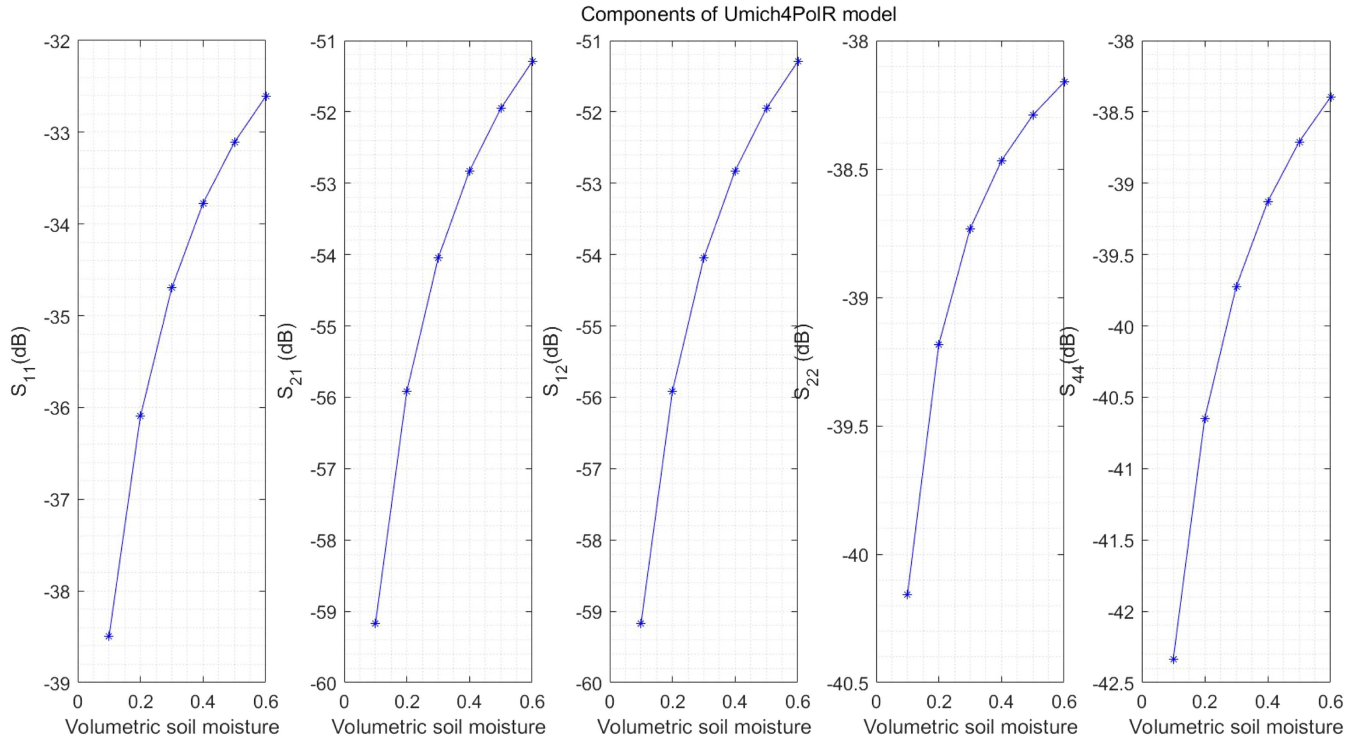

Fig. 4. Modified Mueller matrix elements of S_{11}, S_{21}, S_{12}, S_{22}, and S_{44} versus soil moisture content.

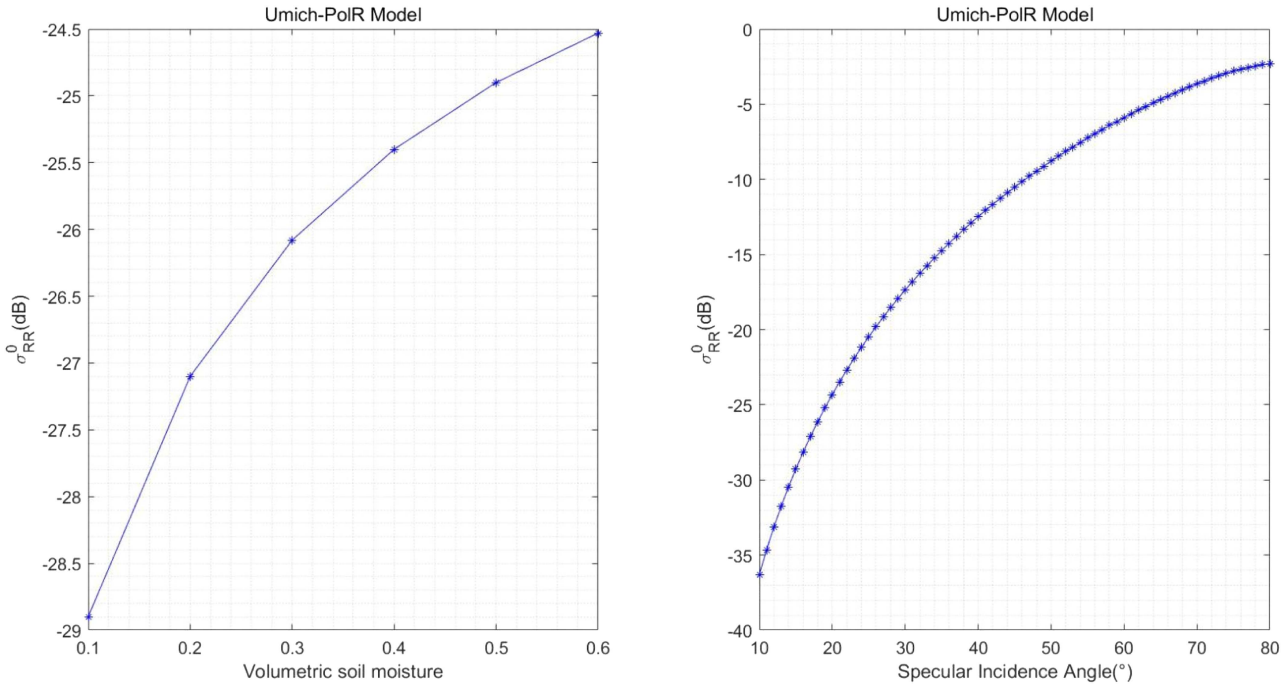

Fig. 5. Specular reflectivity at RR polarization versus soil moisture content (left figure) and specular incidence angle (right figure).

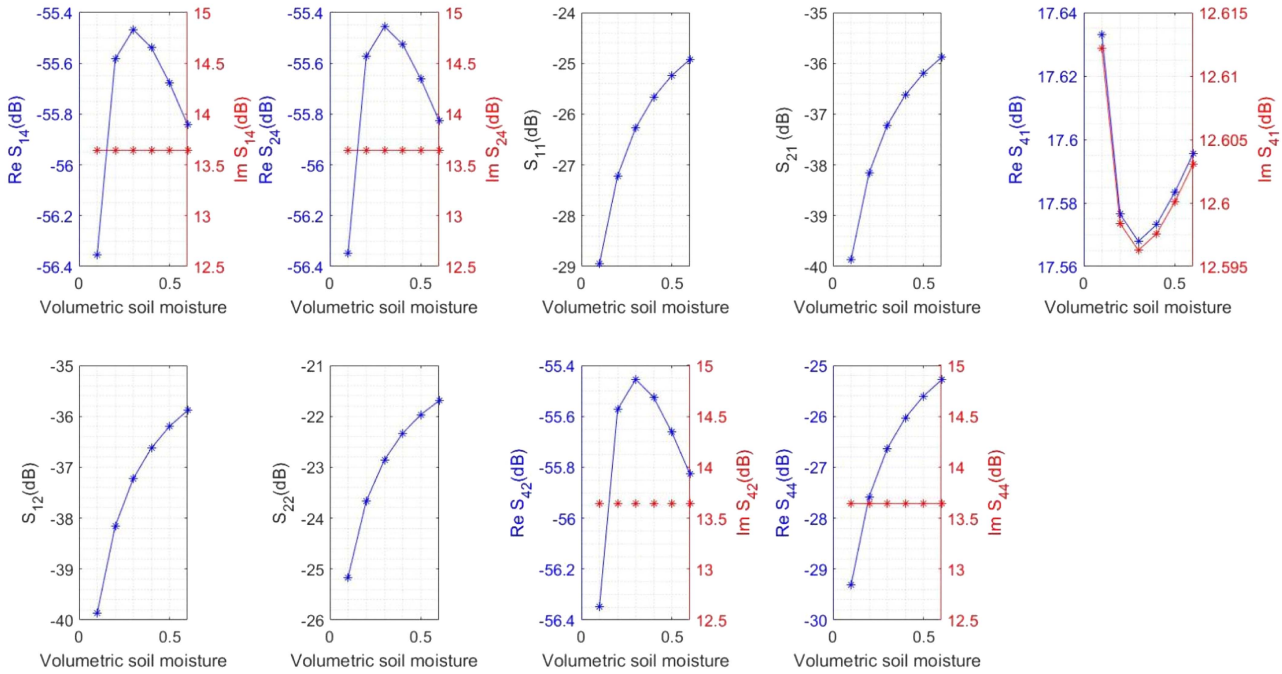

Fig. 6. Modified Mueller matrix elements of P_{14}, P_{24}, P_{11}, P_{21}, P_{41}, P_{12}, P_{22}, P_{42}, and P_{44} versus soil moisture content.

From (22) to (24), we can see that nine elements in the modified Mueller matrix are employed, while their effects versus soil moisture content are different. The trends for S_{14}, S_{24}, and S_{42} are almost the same, although the magnitudes of them are different. For the real parts of S_{14}, S_{24}, and S_{42}, they increase as the soil moisture content increases (when the soil moisture content is lower than 0.3) and the trends become opposite as the soil moisture content is larger than 0.3, while the imaginary parts remain as constants for these three elements. The elements of S_{11}, S_{21}, S_{12}, and S_{22} are not complex numbers but real numbers, while the trends for these four elements increase as the soil moisture content increases. S_{41} and S_{44} are also complex numbers, and their real part and imaginary part of S_{41} decrease as soil moisture content increases (when the soil moisture content

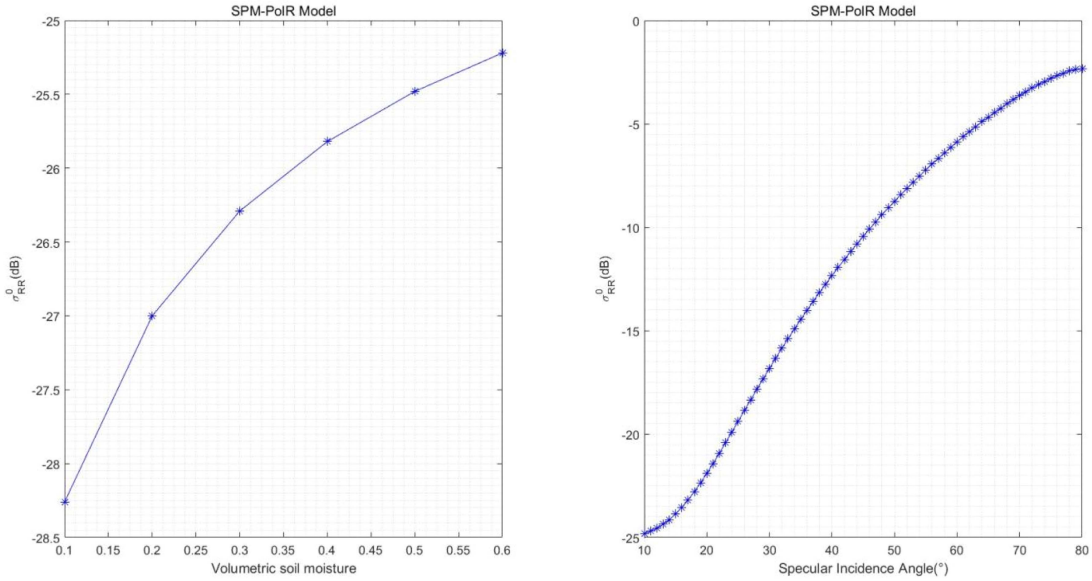

Fig. 7. Specular reflectivity at RR polarization versus soil moisture content (left figure) and specular incidence angle (right figure).

is lower than 0.3) and they increase as soil moisture content increases (when soil moisture content is larger than 0.3). The element of S_{44} is also a complex number, while the real part of S_{44} increases as the soil moisture content increases and the imaginary parts of S_{44} remain as constant for different soil moisture contents.

The final RR reflectivity is the combined actions of these nine elements, and their trends versus soil moisture content and incidence angles are presented in Fig. 7.

We can see from Fig. 7 that RR reflectivity increases as the soil moisture content and incidence angle increase. These trends are consistent with the measured data.

IV. Discussion and Conclusion

From the numerical simulation, as presented in Section III, we can see that, based on the theory and methodology presented in Section II, three models have been developed, i.e., Spec4PolR, Umich4PolR, and SPM4PolR. We can see that the RR scattering coefficient of the Spec4PolR model decreases as the soil moisture content increases and this is contrary to the actual measurement situation; the reasons are due to the too simple assumption during the calculations, as presented by the commonly used Fresnel combination form.

While as for the other two proposed models, i.e., Umich4PolR and SPM4PolR. The trends of RR scattering coefficients versus soil moisture content and specular incidence angles are consistent with the measurement data. The reasons are due to the more complex and more detailed description of the Mueller matrix. One point that should be mentioned is that the incidence angles and soil texture information for the left figure in Figs. 5 and 6are the same, However, the range of RR reflectivity for Umich4PolR is between -29 and -24.5 dB, the one for SPM4PolR is between -28.3 and -25.3 dB. The dynamic variation range for Umich4PolR and SPM4PolR has a slight no more than 0.5 dB difference. The angle variation range for Umich4PolR and SPM4PolR is presented in the right figure of Figs. 5 and 6. From the simulations, we can see that the dynamic range of Umich4PolR is between -37 and -3 dB, while the one for SPM4PolR is between -25 and -3 dB. The results show that the range for the Umich4PolR model seems larger than the one of SPM4PolR. The reasons for this phenomenon are perhaps due to the applicable range of surface roughness. The surface roughness parameters used in the SPM4PolR model are: rms height equals 0.85 cm, and the correlation length is 2.75 cm. While the ones employed for the calculations of the Umich4PolR model are different, the rms height is 1.45 cm and the correlation length is 1.75 cm. For the different surface roughness, they will present different reflectivity properties at different incidence angles. With the development of the GNSS-R or SoOP-R remote sensing technique, its employment of polarization properties will become more and more important, especially RR polarization, which is orthogonal polarization of the present commonly used LR polarization. A companion experiment related to polarization GNSS-R will be conducted in the following month. It should be noted that, although the current models used in this article have not been validated with in situ measurements, they were developed based on the Mueller matrix by changing the modified Stokes vectors to obtain the scattering properties at RR polarization. In other words, if we set the modified Stokes vectors to linear polarization configurations, we can obtain the VV, HH, VH, or HV scattering coefficients, which are compared with the results of traditional models with good consistency. This way, we validate our models and ensure their reliability. The development of the formula for RR polarization calculation in this article will benefit the following polarization study and geophysical parameters retrieval based on RR polarization.

References

[1] A. M. Balakhder, M. M. Al-Khaldi, and J. T. Johnson, "On the coherency of ocean and land surface specular scattering for GNSS-R and signals of opportunity systems," *IEEE Trans. Geosci. Remote Sens.*, vol. 57, no. 12, pp. 10426–10436, Dec. 2019, doi: 10.1109/TGRS.2019.2935257.

[2] M. Kurum, M. Deshpande, A. T. Joseph, P. E. O'Neill, R. H. Lang, and O. Eroglu, "SCoBi-veg: A generalized bistatic scattering model of reflectometry from vegetation for signals of opportunity applications," *IEEE Trans. Geosci. Remote Sens.*, vol. 57, no. 2, pp. 1049–1068, Feb. 2019, doi: 10.1109/TGRS.2018.2864631.

[3] C. D. Hall and R. A. Cordey, "Multistatic scatterometry," in *Proc. Int. Geosci. Remote Sens. Symp., 'Remote Sens., Moving Toward 21st Century'*, 1988, pp. 561–562.

[4] M. C. Evans and C. S. Ruf, "Toward the detection and imaging of ocean microplastics with a spaceborne radar," *IEEE Trans. Geosci. Remote Sens.*, vol. 60, Jun. 2022, Art. no. 4202709, doi: 10.1109/TGRS.2021.3081691.

[5] D. Pascual, M. P. Clarizia, and C. S. Ruf, "Spaceborne demonstration of GNSS-R scattering cross section sensitivity to wind direction," *IEEE Geosci. Remote Sens. Lett.*, vol. 19, Jan. 2022, Art. no. 8006005, doi: 10.1109/LGRS.2021.3049526.

[6] E. Cardellach, Y. Nan, W. Li, R. Padullés, S. Ribó, and A. Rius, "Variational retrievals of high winds using uncalibrated CyGNSS observables," *Remote Sens.*, vol. 12, no. 23, 2020, Art. no. 3930.

[7] W. Li, E. Cardellach, F. Fabra, S. Ribó, and A. Rius, "Assessment of spaceborne GNSS-R ocean altimetry performance using CYGNSS mission raw data," *IEEE Trans. Geosci. Remote Sens.*, vol. 58, no. 1, pp. 238–250, Jan. 2020, doi: 10.1109/TGRS.2019.2936108.

[8] S. Leidner, B. Annane, B. McNoldy, R. Hoffman, and R. Atlas, "Variational analysis of simulated ocean surface winds from the cyclone global navigation satellite system (CYGNSS) and evaluation using a regional OSSE," *J. Atmos. Ocean. Technol.*, vol. 35, pp. 1571–1584, 2018, doi: 10.1175/JTECH-D-17-0136.1.

[9] H. Kim and V. Lakshmi, "Use of cyclone global navigation satellite system (CyGNSS) observations for estimation of soil moisture," *Geophysical Res. Lett.*, vol. 45, no. 16, pp. 8272–8282, Aug. 2018.

[10] D. R. Boyd et al., "Cramer–Rao lower bound for SoOp-R-based root-zone soil moisture remote sensing," *IEEE J. Sel. Topics Appl. Earth Observ. Remote Sens.*, vol. 13, pp. 6101–6114, Oct. 2020, doi: 10.1109/JSTARS.2020.3029158.

[11] S. H. Yueh, R. Shah, M. J. Chaubell, A. Hayashi, X. Xu, and A. Colliander, "A semiempirical modeling of soil moisture, vegetation, and surface roughness impact on CYGNSS reflectometry data," *IEEE Trans. Geosci. Remote Sens.*, vol. 60, Nov. 2022, Art. no. 5800117, doi: 10.1109/TGRS.2020.3035989.

[12] F. Chen, F. Guo, L. Liu, and Y. Nan, "An improved method for pan-tropical above-ground biomass and canopy height retrieval using CYGNSS," *Remote Sens.*, vol. 13, no. 13, Jun. 2021, Art. no. 2491.

[13] R. Shah, T. Freeman, and J. L. Garrison, "Constellations of CubeSats to exploit signals-of-opportunity for Earth system science," *Proc. SPIE*, vol. 10769, 2018, Art. no. 107690D, doi: 10.1117/12.2319863.

[14] V. U. Zavorotny and A. G. Voronovich, "Scattering of GPS signals from the ocean with wind remote sensing application," *IEEE Trans. Geosci. Remote Sens.*, vol. 38, no. 2, pp. 951–964, Mar. 2000, doi: 10.1109/36.841977.

[15] S. Zhang, Z. Pu, D. J. Posselt, and R. Atlas, "Impact of CYGNSS ocean surface wind speeds on numerical simulations of a hurricane in observing system simulation experiments," *J. Atmos. Ocean. Technol.*, vol. 34, no. 2, pp. 375–383, Feb. 2017.

[16] F. Huang et al., "Spaceborne GNSS reflectometry with Galileo signals on FY-3E/GNOS-II: Measurements, calibration, and wind speed retrieval," *IEEE Geosci. Remote Sens. Lett.*, vol. 20, Feb. 2023, Art. no. 3501505, doi: 10.1109/LGRS.2023.3241358.

[17] C. Chew and E. Small, "Description of the UCAR/CU soil moisture product," *Remote Sens.*, vol. 12, no. 10, 2020, Art. no. 1558.

[18] B. Liu et al., "Statistical analysis of CyGNSS speckle and its applications to surface water mapping," *IEEE Trans. Geosci. Remote Sens.*, vol. 60, Aug. 2022, Art. no. 5803915, doi: 10.1109/TGRS.2022.3196012.

[19] V. Zavorotny et al., "Seasonal polarimetric measurements of soil moisture using tower-based GPS bistatic radar," in *Proc. IEEE Int. Geosci. Remote Sens. Symp.*, 2003, vol. 2, pp. 781–783.

[20] N. Rodriguez-Alvarez, S. Misra, and M. Morris, "The polarimetric sensitivity of SMAP-reflectometry signals to crop growth in the U.S. corn belt," *Remote Sens.*, vol. 12, no. 6, 2020, Art. no. 1007.

[21] H. Carreno-Luengo, S. Lowe, C. Zuffada, S. Esterhuizen, and S. Oveisgharan, "Spaceborne GNSS-R from the SMAP mission: First assessment of polarimetric scatterometry over land and cryosphere," *Remote Sens.*, vol. 9, no. 4, 2017, Art. no. 362.

[22] M. J. Unwin et al., "An introduction to the HydroGNSS GNSS reflectometry remote sensing mission," *IEEE J. Sel. Topics. Appl. Earth Observ. Remote Sens.*, vol. 14, pp. 6987–6999, Jun. 2021, doi: 10.1109/JSTARS.2021.3089550.

[23] X. Wu and S. Jin, "Models and theoretical analysis of SoOp circular polarization bistatic scattering for random rough surface," *Remote Sens.*, vol. 12, no. 9, 2020, Art. no. 1506.

[24] X. Wu, Y. Song, J. Xu, Z. Duan, and S. Jin, "Bistatic scattering simulations of circular and linear polarizations over land surface for signals of opportunity reflectometry," *Geosci. Lett.*, vol. 8, no. 1, 2021, Art. no. 11, doi: 10.21203/rs.3.rs-117659/v1.

[25] X. Wu and S. Jin, "GNSS-reflectometry: Forest canopies polarization scattering properties and modeling," *Adv. Space Res.*, vol. 54, no. 5, pp. 863–870, 2014.

[26] M. Shah et al., "Seismo ionospheric anomalies in Turkey associated with $M \geq 6.0$ earthquakes detected by GPS stations and GIM TEC," *Adv. Space Res.*, vol. 65, no. 11, pp. 2540–2550, 2020, doi: 10.1016/j.asr.2020.03.005.

[27] A. Fung and H. Eom, "Coherent scattering of a spherical wave from an irregular surface," *IEEE Trans. Antennas Propag.*, vol. 31, no. 1, pp. 68–72, Jan. 1983, doi: 10.1109/TAP.1983.1142979.

[28] C. Yin, "Soil moisture remote sensing with global navigation satellite system reflectometry," Ph.D. dissertation, Nanjing Univ. Inf. Sci. Technol., Nanjing, China, 2019, doi: 10.27248/d.cnki.gnjqc.2019.000704.

[29] F. T. Ulaby and C. Elachi, "Radar polarimetry for geoscience applications," Apr. 1990.

[30] P. Liang, L. E. Pierce, and M. Moghaddam, "Radiative transfer model for microwave bistatic scattering from forest canopies," *IEEE Trans. Geosci. Remote Sens.*, vol. 43, no. 11, pp. 2470–2483, Nov. 2005, doi: 10.1109/TGRS.2005.853926.

[31] Y. Oh, K. Sarabandi, and F. T. Ulaby, "An empirical model and an inversion technique for radar scattering from bare soil surfaces," *IEEE Trans. Geosci. Remote Sens.*, vol. 30, no. 2, pp. 370–381, Mar. 1992, doi: 10.1109/36.134086.

[32] J. A. Kong, R. T. Shin, and L. Tsang, *Theory of Microwave Remote Sensing*, vol. 2. Hoboken, NJ, USA: Wiley, Jul. 1985.

Xuerui Wu received the Ph.D. degree in land surface theoretical modelling and applications of GNSS-reflectometry from Dalian Maritime University, Dalian, China, in 2012.

From 2013 to 2014, she was a Postdoctor with Shanghai Astronomical Observatory, Chinese Academy of Sciences, Shanghai, China, where she is currently an Associate Professor. Her research activities are related to GNSS-reflectometry and hydrology. She has concentrated on the topic of GNSS-R land surface scattering models since she was a Ph.D. student in 2009.

Lixiong Chen received the Ph.D. degree in electromagnetic field and microwave technology from the Shanghai Institute of Technical Physics, Shanghai, China, in 2011.

He is currently a Lecturer with Shanghai Maritime University, Shanghai, China. His research activities are related to navigational meteorology and oceanography.

Jiancheng Shi (Fellow, IEEE) received the B.A. degree in microwave remote sensing from the University of Lanzhou, Lanzhou, China, in 1982, and the M.A. and Ph.D. degrees in geography from the University of California, Santa Barbara, CA, USA, in 1987 and 1991, respectively.

He is currently with the National Space Science Centers, Chinese Academic of Sciences, Beijing, China, as a Research Scientist. His research interests include microwave modeling of snow and soil signatures, image processing and analysis, and inversion models for retrieving physical parameters from remote sensing data.